

# Effects of annealing atmosphere on microstructure, electrical properties and domain structure of BiFeO<sub>3</sub> thin films

Yuanyang Sun<sup>1</sup> · Wei Cai<sup>1,2</sup> · Rongli Gao<sup>1,2</sup> · Xianlong Cao<sup>1,2</sup> · Fengqi Wang<sup>1</sup> · Tianyu Lei<sup>1</sup> · Xiaoling Deng<sup>1,2</sup> · Gang Chen<sup>1,2</sup> · Haifeng He<sup>1</sup> · Chunlin Fu<sup>1,2</sup>

Received: 14 February 2017 / Accepted: 24 April 2017 / Published online: 3 May 2017  
© Springer Science+Business Media New York 2017

**Abstract** Bismuth ferrite thin films were prepared by sol–gel method and spin-coating technique. The effects of annealing atmosphere (air and oxygen) on the microstructure, dielectric, ferroelectric properties and domain structure of bismuth ferrite thin films have been studied systematically. The XRD and AFM results indicate that the bismuth ferrite thin films annealed in air and oxygen atmosphere are rhombohedral perovskite structure and bismuth ferrite thin films annealed in oxygen atmosphere have higher purity, better thickness uniformity and smoothness, and slightly larger grain size than that of the sample annealed in air. Bismuth ferrite annealed in oxygen atmosphere have higher dielectric constant, lower dielectric loss and much higher remnant polarization than that of the thin films annealed in air. The PFM (Piezoelectric Force Microscopy) results indicate that there are coexistence of single domain and polydomain state grains in bismuth ferrite annealed in air and oxygen atmosphere, and the single domain critical size is 80–100 and 100–110 nm respectively. Moreover, there are non-neutral domain wall (negatively charged “tail to tail” and positively charged “head to head” domain wall) in bismuth ferrite thin films annealed in air and oxygen atmosphere.

## 1 Introduction

In recent years, multiferroic materials with the coexistence of at least two ferroic orders (ferroelectric, (anti-)ferromagnetic and ferroelastic) have gained widely attention because of the coupling between electric and magnetic ferroic orders (magnetoelectric coupling). The characteristic makes it possible to control ferroelectric polarization with magnetic field or to control magnetism by electric field, which is potential for spintronic devices, multi-state memories, magnetoelectric devices and so on [1–3]. Bismuth ferrite (BiFeO<sub>3</sub>, short for BFO) is the most popular room-temperature single phase multiferroic materials, which has high Curie temperature ( $T_C \sim 830^\circ\text{C}$ ) and Néel temperature ( $T_N \sim 370^\circ\text{C}$ ) [4–6]. But the practical applications of BFO have been restricted owing to two reasons. On the one hand, it is difficult to synthesize single phase BFO because that the volatilization of Bi<sub>2</sub>O<sub>3</sub> and phase decomposition at high temperature fabrication process are prone to result in some impurity phases such as Bi<sub>2</sub>Fe<sub>4</sub>O<sub>9</sub>, Bi<sub>25</sub>FeO<sub>40</sub> [7]. On the other hand, the leakage current of BFO materials is higher as a result of the existence of Fe<sup>2+</sup> and oxygen vacancies ( $V_O^x + 2Fe^{3+} \rightarrow V_O^{\cdot\cdot} + 2Fe^{2+}$ ) [8]. In order to obtain single phase BFO thin films with excellent ferroelectricity and low leakage current, several attempts such as ion substitution [9–14], introduction of buffer layer [15, 16], epitaxy [17], control of thickness [18, 19] have been conducted. Moreover, the heat treatment in oxygen atmosphere for BFO materials can inhibit the formation of oxygen vacancy and make its leakage current decrease in theory so as to enhance its ferroelectricity based on the above analysis. Go et al. [20] found that the BFO thin films annealed in O<sub>2</sub> have higher remnant polarization and lower leakage current. Prashanthi et al. [21] found that the BFO thin films annealed in O<sub>2</sub> is single phase and have more sufficient

✉ Wei Cai  
caiwei\_cqu@163.com

✉ Chunlin Fu  
chl fu@126.com

<sup>1</sup> School of Metallurgy and Materials Engineering, Chongqing University of Science and Technology, University Town, Shapingba District, Chongqing 401331, People's Republic of China

<sup>2</sup> Chongqing Key Laboratory of Nano/Micro Composite Material and Device, Chongqing 401331, People's Republic of China

crystallinity and lower surface roughness compared with the samples annealed in air and nitrogen, and XPS results confirmed that the Fe ion of BFO thin films annealed in O<sub>2</sub> is 3+ valence state, and the Fe ion of the films annealed in air and nitrogen is mainly 2+ valence state. But Singh et al. [22] prepared BFO thin films in various atmosphere (oxygen, air and nitrogen) and found that the films annealed in nitrogen have lower leakage, better ferroelectric and magnetic properties than that of the samples annealed in air and oxygen. The ferroelectric and magnetic properties of the sample annealed in air are better than that of the sample annealed in oxygen, but the leakage current of the sample annealed in oxygen is lower. Liu et al. [23] sintered BFO ceramics in H<sub>2</sub>, Air and O<sub>2</sub> respectively and found that the sample sintered in H<sub>2</sub> atmosphere has higher spontaneous polarization, but the spontaneous polarization of the sample sintered in O<sub>2</sub> atmosphere is the lowest. Moreover, Simões et al. [24] found BFO thin films annealed in air has lower leakage current and superior ferroelectric property to the sample annealed in oxygen. The similar results have been gotten by Kim et al. [25]. As mentioned above, the effects of annealing atmosphere (especially air and oxygen) on phase formation and electric properties of BFO thin films are controversial. Meanwhile, the ferroelectric domain of BFO thin films is an intrinsic critical factor that influences its electric properties, and the effect of annealing atmosphere on domain structure has not been done systematically. Thus, we fabricated BFO thin films in different annealing atmosphere (air and oxygen) and studied systematically the effects of annealing atmosphere on crystal structure, surface morphology, dielectric properties, ferroelectric properties and domain structure.

## 2 Experimental procedure

The BFO thin films were prepared by sol–gel method and spin-coating technique. Bismuth nitrate ([Bi(NO<sub>3</sub>)<sub>3</sub>·5H<sub>2</sub>O], 99.5%) and iron nitrate ([Fe(NO<sub>3</sub>)<sub>3</sub>·9H<sub>2</sub>O], 99.5%) were used as raw materials. 2-methoxyethanol ([HOCH<sub>2</sub>CH<sub>2</sub>OCH<sub>3</sub>], 99.5%) and acetic acid ([CH<sub>3</sub>COOH]), 99.5%, were used as mixed solvent (the volume ratio of 2-methoxyethanol to acetic acid was 2:1). Firstly, the solution were prepared by adding bismuth nitrate and iron nitrate in the molar ratio of Bi: Fe = 1.1:1 (excess of Bi to compensate its loss during annealing process) to the mixed solvent and the solution was continuously stirred at 20 °C for 30 min to ensure complete dissolution of bismuth nitrate and iron nitrate. Secondly, acetic anhydride ([C<sub>4</sub>H<sub>6</sub>O<sub>3</sub>], 99.5%) as dehydrating agent was added to the solution. It is noteworthy that citric acid ([C<sub>6</sub>H<sub>8</sub>O<sub>7</sub>], 99.5%, the molar ratio of citric acid to metallic cation is 1:1) as a chelating agent should be added when

the temperature of solution decreases to 25 °C, which is because that the exothermal dehydration reaction can result in the sharp rise of temperature easy to produce precipitation. Moreover, the viscosity of the solution was adjusted by adding ethanol amine ([C<sub>2</sub>H<sub>7</sub>NO], 99.5%). Finally, a certain amount of 2-methoxyethanol was added to adjust the concentration of the solution to be 0.3 mol/L. And then the transparent and reddish-brown precursor solution was obtained after stirring and aging for 48 h at 25 °C. The amorphous films were deposited on the Pt(100 nm)/Ti(30 nm)/SiO<sub>2</sub>(500 nm)/Si(500 μm) substrate by spin-coating technique at 3000 rpm for 20 s by spin processor. After spin coating, the films were annealed in different atmosphere (air and oxygen) in conventional tube furnace at 600 °C for 15 min respectively. To obtain the desired thickness of thin films, the processes of spin coating and annealing were repeated several times.

The phase analysis of the films were performed at room temperature by X-ray diffraction (DX-2700 model, Dandong Fangyuan, China, Cu K<sub>α</sub>). The thickness of thin films is about 300 nm examined in a stylus profiler (P-7, KLA-Tencor, USA). The Au top electrode with a diameter of 200 μm and a thickness of 50 nm was deposited on the thin films by DC magnetron sputtering (JGP280, SKY, China). The room temperature ferroelectric hysteresis loops of thin films were measured by ferroelectric test system (TF2000E, aixACCT, Germany). The room-temperature capacitance of BFO films was determined by impedance analyzer (LCR, HP 4980 A, Agilent, USA). The dielectric constant was calculated by the following equation:

$$\epsilon = Ct/\epsilon_0 A \quad (1)$$

where  $C$  is the capacitance (F),  $\epsilon_0$  is the free space dielectric constant value ( $8.85 \times 10^{-12}$  F/m),  $A$  represents the capacitor area (m<sup>2</sup>) and  $t$  represents the thickness (m) of the films. The surface morphology and domain structure of BFO thin films were obtained in AFM (Atomic Force Microscopy) mode and PFM (Piezoelectric Force Microscopy, 3 V AC voltage is applied on tip) mode by scanning probe microscopy (NTEGRA Prima, NT-MDT, Russia). Tip was CSG01 type (PtIr coated with radii of about 10 nm, resonant frequency of 9.8 kHz, and spring constant of 0.03 N/m, NT-MDT, Russia).

## 3 Results and discussion

### 3.1 Microstructure

X-ray diffraction patterns of BFO thin films annealed in air and oxygen atmosphere are shown in Fig. 1. The refinement of crystal structure has been done by Jade 6.0 software. Table 1 shows the lattice constants of BFO thin films.

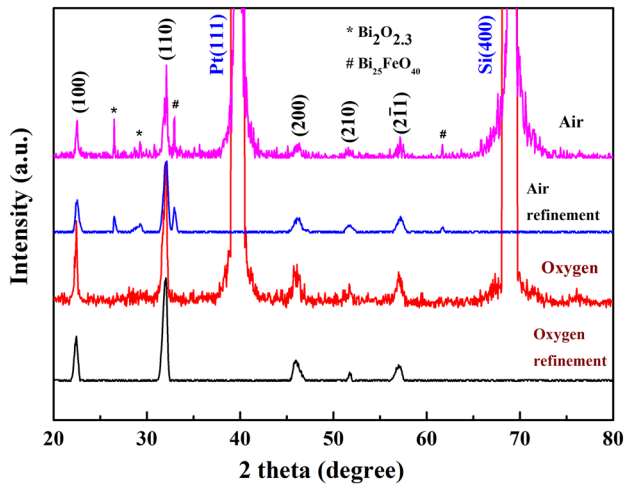


**Fig. 1** XRD patterns of BFO thin films annealed in different atmosphere

Firstly, the main phase of the thin films annealed in air and oxygen atmosphere is BFO phase (*R3m* group, JCPDS Card No. 72-2112). But there are some diffraction peaks around 26.5°, 29.3° and 33°, 62° which belong to impurity ( $\text{Bi}_2\text{O}_{2.3}$  and  $\text{Bi}_{25}\text{FeO}_{40}$ ) in the sample annealed in air, which may result from the kinetics of phase formation influenced by the annealing atmospheres. According to the intensity of diffraction peaks of BFO phase, it is found that the thin films annealed in oxygen atmosphere is single BFO phase and have more sufficient crystallinity than that of the sample annealed in air, which indicates that oxygen annealing atmosphere is more beneficial to improve the crystallinity and purity. To obtain the purity of BFO thin films, the XRD quantitative analysis was done. The mass fraction of BFO phase was calculated by the equation as follows:

$$W_{\text{BFO}} = \frac{I_{\text{BFO}}}{I_{\text{BFO}} + \sum_{i=1}^n \frac{I_{X_i} K_{\text{BFO}}}{K_{X_i}}} \quad (2)$$

where  $W_{\text{BFO}}$  is the mass fraction of BFO,  $n$  is the number of impurity phase.  $I_{\text{BFO}}$  and  $I_{X_i}$  are the intensity of reflection of (*hkl*) in BFO and the impurity phase ( $\text{Bi}_{25}\text{FeO}_{40}$  and  $\text{Bi}_2\text{O}_{2.3}$ ), respectively.  $K_{\text{BFO}}$  (8.89),  $K_{X_1}$  (5.91) and  $K_{X_2}$  (6.94) are the *RIR* value of  $\text{BiFeO}_3$ ,  $\text{Bi}_{25}\text{FeO}_{40}$ , and  $\text{Bi}_2\text{O}_{2.3}$ , respectively. The mass fraction of BFO phase annealed in

air and oxygen atmosphere by Eq. (2) is 88.7 and 97.6% respectively, which indicates that the thin films annealed in oxygen atmosphere approach to single phase. Secondly, the lattice constant and rhombohedral angle of the sample annealed in oxygen atmosphere are larger than that of the sample annealed in air (shown in Table 1).

Figure 2 shows the surface morphology of BFO thin films annealed in air and oxygen atmosphere. Firstly, it is observed that both of BFO thin films are smooth, dense and uniform. The average grain size of the sample annealed in air and oxygen atmosphere is 64 and 72 nm respectively. Our results are different from Prashanthi’s results [21]. In Prashanthi’s work, they found that the average grain size of BFO thin films annealed in  $\text{O}_2$  was smaller than that of the films annealed in air, which may be due to creation of oxygen vacancies which affect grain growth by changing the diffusion flux of oxygen vacancy [21, 24]. The reason for our different results is unclear. Secondly, the root mean square roughness (RMS) of BFO thin films annealed in air and oxygen atmosphere is 9.019 and 7.509 nm respectively, indicating that annealing in oxygen atmosphere can enhance the thickness uniformity. In summary, annealing in oxygen atmosphere is more beneficial to form single phase BFO thin films with good thickness uniformity and smoothness.

### 3.2 Electric properties

#### 3.2.1 Dielectric properties

The frequency dependences of the dielectric properties of BFO thin films annealed in different atmosphere at room temperature are shown in Fig. 3. Firstly, it is evident that the dielectric constant of BFO thin films annealed in air and oxygen atmosphere decreases with increasing frequency. The behavior of dielectric constant with frequency is attributed to the fact that the electric dipoles are not able to catch up with the change of AC electric field at higher frequency, thus leading to relaxation phenomenon. Secondly, the dielectric constant of BFO thin films annealed in oxygen atmosphere is higher than that of the films annealed in air, which may result from two reasons. On the one hand, the average grain size of BFO thin films annealed in oxygen atmosphere is larger than that of the films annealed in air. It is well known that the dielectric constant of ferroelectric

**Table 1** Crystal structure of BFO thin films annealed in different atmosphere

Annealing atmosphere	Lattice parameters			Crystal structure	Rhombohedral angle (°)
	<i>a</i> (nm)	<i>b</i> (nm)	<i>c</i> (nm)		
Air	0.3948	0.3948	0.3948	Rhombohedral (PDF No. 72-2112)	89.4
Oxygen	0.3994	0.3994	0.3994	Rhombohedral (PDF No. 72-2112)	89.86

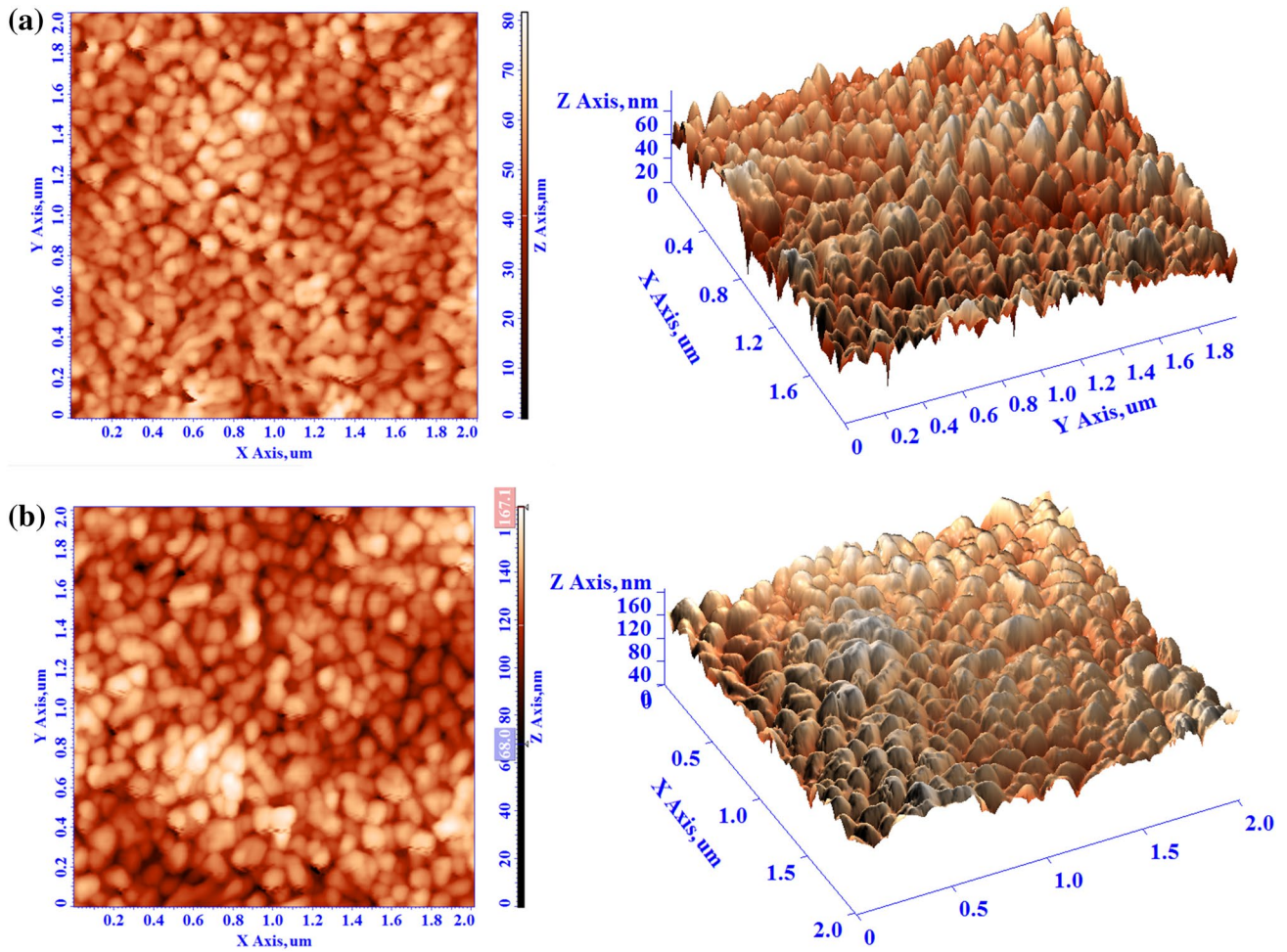


**Fig. 2** AFM images of BFO thin films annealed in **a** air and **b**  $O_2$

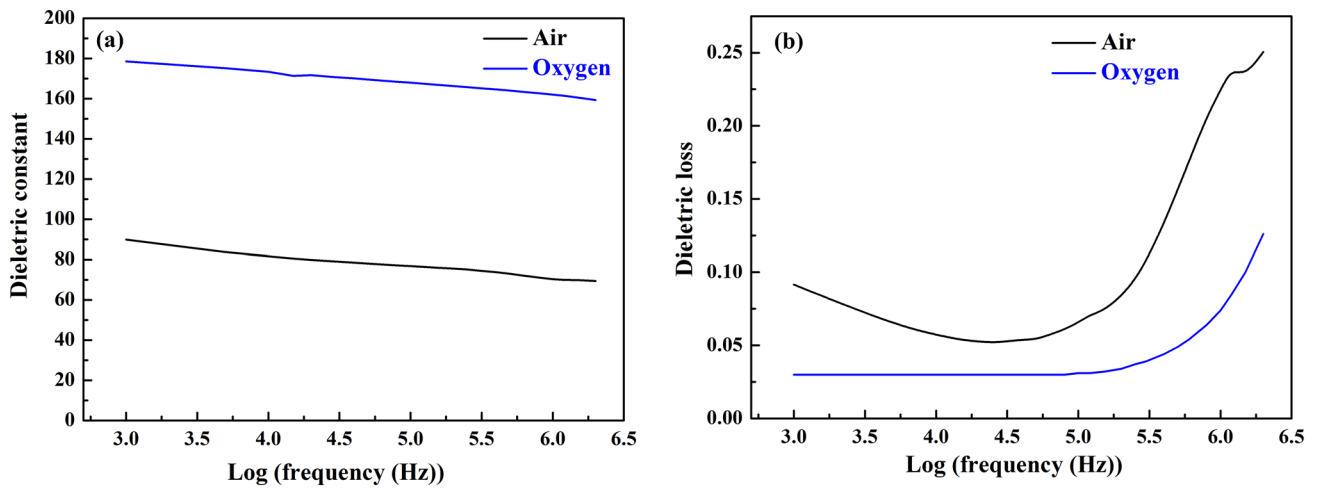


**Fig. 3** Frequency dependences of dielectric properties of BFO thin films annealed in different atmosphere **a**  $\epsilon-\log(f)$ , **b**  $\tan\delta-\log(f)$

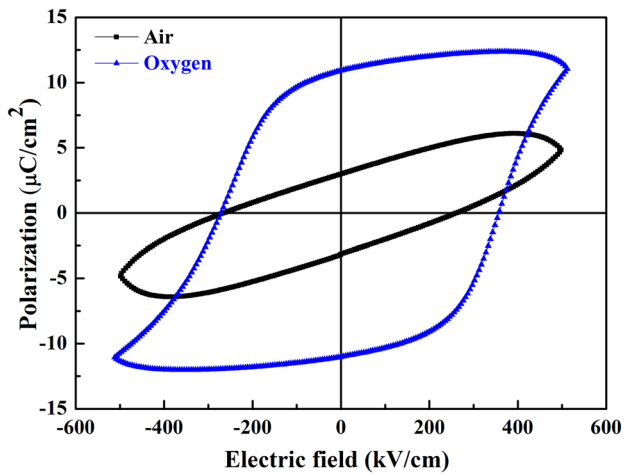


**Fig. 4** Room temperature hysteresis loops of BFO thin films annealed in different atmosphere measured at 3 kHz

**Table 2** The remnant polarization ( $2P_r$ ) and coercive electric field ( $2E_C$ ) of BFO thin films annealed in different atmosphere

Annealing atmosphere	$2P_r$ ( $\mu\text{C}/\text{cm}^2$ )	$2E_C$ (kV/cm)
Air	6.16	516.49
Oxygen	21.92	634.92

grain in is higher than that of non ferroelectric grain boundary, which indicates that the dielectric constant of BFO thin films with larger grain size is higher. On the other hand, the existence of impurity phases in the films annealed in air may result in its lower dielectric constant. Thirdly, the dielectric loss of BFO thin films annealed in oxygen atmosphere is lower than that of the films annealed in air, which can be due to the lower oxygen vacancy concentration and higher purity of BFO phase in the sample annealed in oxygen atmosphere [22, 26]. Moreover, the dielectric loss of BFO thin film annealed in oxygen atmosphere keeps almost constant when frequency is lower than 1 MHz and then increases at higher frequency. But the dielectric loss of the sample annealed in air decreases firstly and then increases as frequency increases.

### 3.2.2 Ferroelectric properties

The room temperature hysteresis loops of BFO thin films annealed in air and oxygen atmosphere measured at 3 kHz are shown in Fig. 4. The remnant polarization ( $P_r$ ) and coercive electric field ( $E_C$ ) are listed in Table 2. Firstly, the hysteresis loops of BFO films annealed in air are unable

to reach a fully saturated state, and the hysteresis loops of BFO films annealed in oxygen atmosphere show well-saturated characteristics. It may result from relatively more oxygen vacancies of BFO thin films annealed in air caused by the volatilization of Bi and reduction of  $\text{Fe}^{3+}$  during annealing process. Furthermore, the presence of impurity phase ( $\text{Bi}_{25}\text{FeO}_{40}$  and  $\text{Bi}_2\text{O}_{2.3}$ ) in the sample annealed in air may be the other reason. Secondly, the remnant polarization of the sample annealed in oxygen atmosphere is much higher than that of the sample annealed in air, which is attributed to two reasons. On the one hand, the grain boundary is non ferroelectric and the smaller grain size make it difficult to form large ferroelectric domains, which reduces the effective contribution to total polarization so that the remnant polarization of BFO thin films with smaller grain size is lower [27, 28]. As mentioned previously, the grain size of the films annealed in oxygen atmosphere is larger than that of the films annealed in air. On the other hand, the higher purity of BFO thin films annealed in oxygen atmosphere is the important factor. Thirdly, the coercive field of the sample annealed in air is lower than that of the sample annealed in oxygen atmosphere. Moreover, the hysteresis loops of BFO thin films annealed in oxygen atmosphere show obvious asymmetric characteristics in the electric field axis and the loops significantly shift to the positive direction of electric field axis. It suggests that there is obvious internal bias field in the thin films annealed in oxygen atmosphere. The internal bias electric field ( $E_{\text{int}}$ ) can be obtained according to the equation ( $E_{\text{int}} = (E_C^+ - E_C^-)/2$ ,  $E_C^+$  and  $E_C^-$  is the coercive electric field in positive and negative electric field axis respectively).  $E_{\text{int}}$  of the thin films annealed in air and oxygen atmosphere is 3.015 and 43.81 kV/cm respectively. In generally, the asymmetric hysteresis loops in ferroelectric thin films may result from the difference in work functions between the top and bottom electrodes [29] and the imprint phenomenon caused by defect (such as oxygen vacancy) [30]. For the BFO thin films annealed in air with the same electrode configuration (top and bottom electrode is Au and Pt, respectively), the hysteresis loop is almost symmetric along the electric field axis. It suggests that the difference of work function between the bottom and top electrodes (Pt: 5.65 eV, Au: 5.1 eV) is obviously not the main reason. In other words, the defect may be the important reason for asymmetric hysteresis loops in BFO thin films annealed in oxygen atmosphere. As mentioned above, it is easy to form oxygen vacancy during the heat treatment of BFO thin films. Oxygen vacancy ( $V_{\text{O}}^{\bullet\bullet}$ ) or complex defect ( $V_{\text{Bi}}^{\bullet\bullet} - V_{\text{O}}^{\bullet\bullet}$ ) located in the interface between films and electrodes and grain boundary promote local stoichiometry deviation and then result in asymmetric hysteresis loops. That is to say,

the degree of asymmetry of hysteresis loop should enhance with the increasing concentration of oxygen vacancy. However, it is noteworthy that the hysteresis loops of BFO thin films with higher concentration of oxygen vacancy resulting from air annealing is almost symmetric, which may be due to that the applied electric field is not enough to make oxygen vacancy move to form imprint phenomenon in BFO thin films with smaller grain size although the concentration of oxygen vacancy is higher.

### 3.3 Domain structure

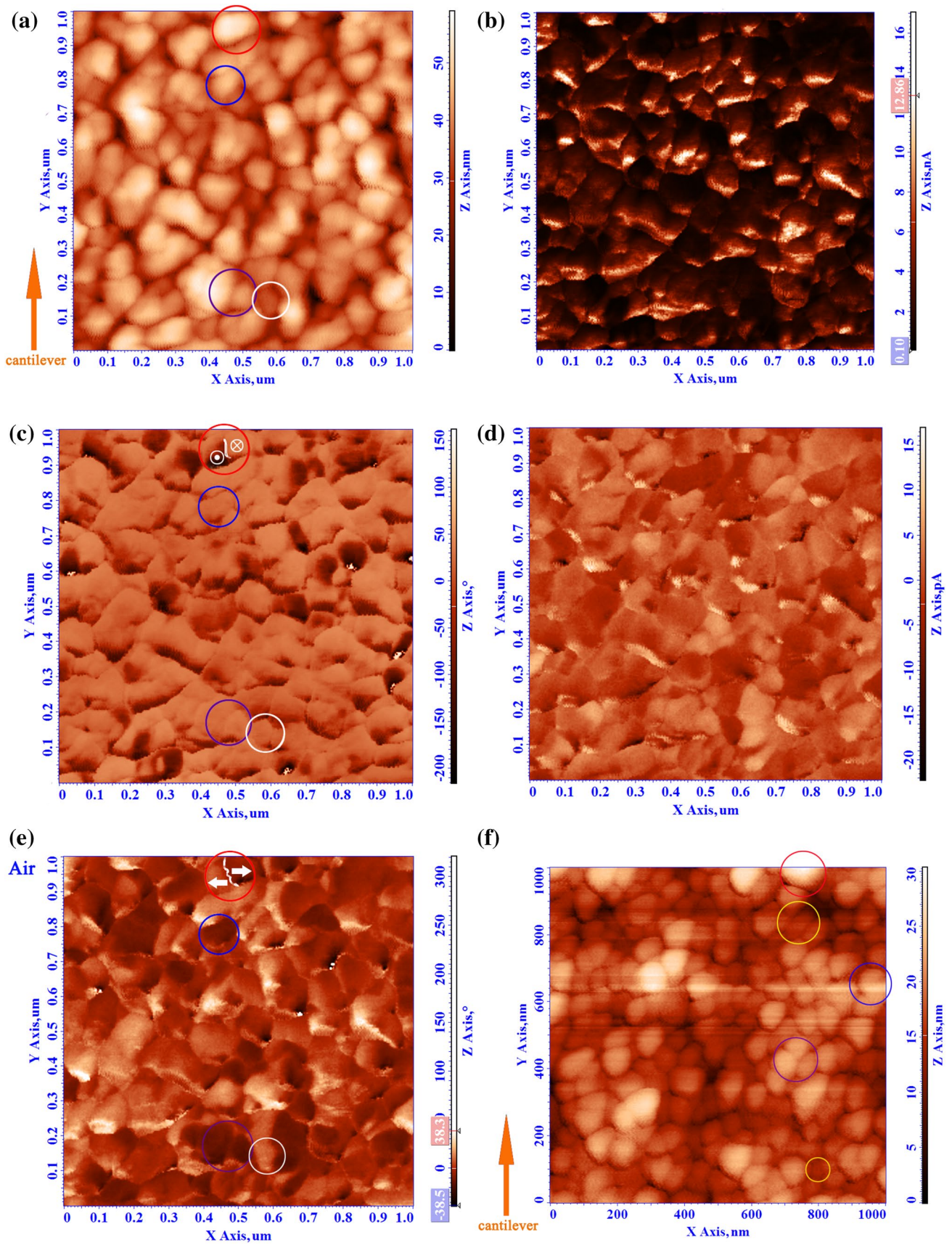
Figure 5 shows the AFM topography and PFM images of BFO thin films annealed in air and oxygen atmosphere. Firstly, the out of plane (OP) and in-plane (IP) phase images of the two thin films show the different phase contrast, indicating the different direction of polarization. It suggests that the polycrystalline BFO thin films annealed in air and oxygen atmosphere are polydomain state. As mentioned above XRD results, two polycrystalline BFO thin films annealed in air and oxygen atmosphere belong to the rhombohedral structure of  $\text{BiFeO}_3$  ( $R3m$ ), indicating that the direction of polarization is  $\langle 111 \rangle$ . The result suggests that the  $\langle 111 \rangle$  polarization should have out-of-plane and in-plane polarization component. In the OP phase image (Fig. 5c, h), the bright region represents the domains with the polarization toward the bottom electrode (the direction of polarization is symbolized by  $\otimes$ ), while the dark region represents the domains with the polarization upward (the direction of polarization is symbolized by  $\odot$ ). In the IP phase image (Fig. 5e, j), the bright region represents the domain with polarization toward the left direction (the direction of polarization is symbolized by  $\leftarrow$ ), and the dark region represents the domain with polarization toward the right direction (the direction of polarization is symbolized by  $\rightarrow$ ). Secondly, it is found that there are single domain state grain (such as the white circle region and blue circle region in Fig. 5a, c, e, and the yellow circle region in Fig. 5f, h, j) and polydomain state grain (such as the red circle region in Fig. 5a, c, e, and the red circle region and blue circle region in Fig. 5f, h, j) in two BFO thin films. According to the grain size of single domain and polydomain state grains, it is concluded that the single domain critical size of BFO thin films annealed in air and oxygen atmosphere is 80–100 and 100–110 nm respectively. Moreover, it is also seen that the domains of some adjacent grains merge into single domain in two samples (such as the purple circle region in Fig. 5a, c, e, f, h, j). Thirdly, it is found that there are some non-neutral domain wall in two BFO thin films. For BFO thin films annealed in air, there

**Fig. 5** Topography (a), OP PFM amplitude (b) and OP phase (c) IP PFM amplitude (d) IP phase (e) images of BFO thin films annealed in air. Topography (f), OP PFM amplitude (g) and OP phase (h) IP PFM amplitude (i) IP phase (j) images of BFO thin films annealed in oxygen atmosphere

is “tail to tail” domain wall (see the red circle region in Fig. 5a, c, e). And for BFO thin films annealed in oxygen atmosphere, there are “tail to tail” domain wall (see the red circle region in Fig. 5f, h, j) and “head to head” domain wall (see the blue circle region in Fig. 5f, h, j). “tail to tail” and “head to head” domain wall is negatively charged and positively charged respectively. Because there are a large number of oxygen vacancies in BFO thin films, BFO thin films show p-type electrical conductivity [29, 30]. Therefore, the majority carriers such as positively charged hole and  $V_o^{\bullet}$  accumulate in “tail to tail” domain wall of p-type BFO thin films.

## 4 Conclusions

In conclusion, BFO thin films were prepared via sol–gel spin-coating method and different annealing atmosphere and its microstructure, dielectric and ferroelectric properties, domain structure have been investigated. The XRD results indicate that the two BFO thin films annealed in air and oxygen atmosphere are rhombohedral perovskite structure, and oxygen atmosphere annealing is more beneficial to form pure BFO phase. According to AFM results, it is found that the BFO thin films annealed in oxygen atmosphere have better thickness uniformity and smoothness, and slightly larger grain size than that of the sample annealed in air. BFO thin films annealed in oxygen atmosphere have higher dielectric constant and lower dielectric loss than that of the sample annealed in air. And the remnant polarization of BFO thin films annealed in oxygen atmosphere is much higher than that of the sample annealed in air. The results suggest that the dielectric and ferroelectric properties of BFO thin films annealed in oxygen atmosphere are superior to that of thin films annealed in air. The PFM results show that single domain and polydomain state grains coexist in the BFO thin films annealed in air and oxygen atmosphere, and the single domain critical size of BFO thin films annealed in air and oxygen atmosphere is 80–100 and 100–110 nm respectively. Moreover, BFO thin films annealed in air have negatively charged “tail to tail” domain wall, and BFO thin films annealed in oxygen atmosphere have both negatively charged “tail to tail” domain wall and positively charged “head to head” domain wall.



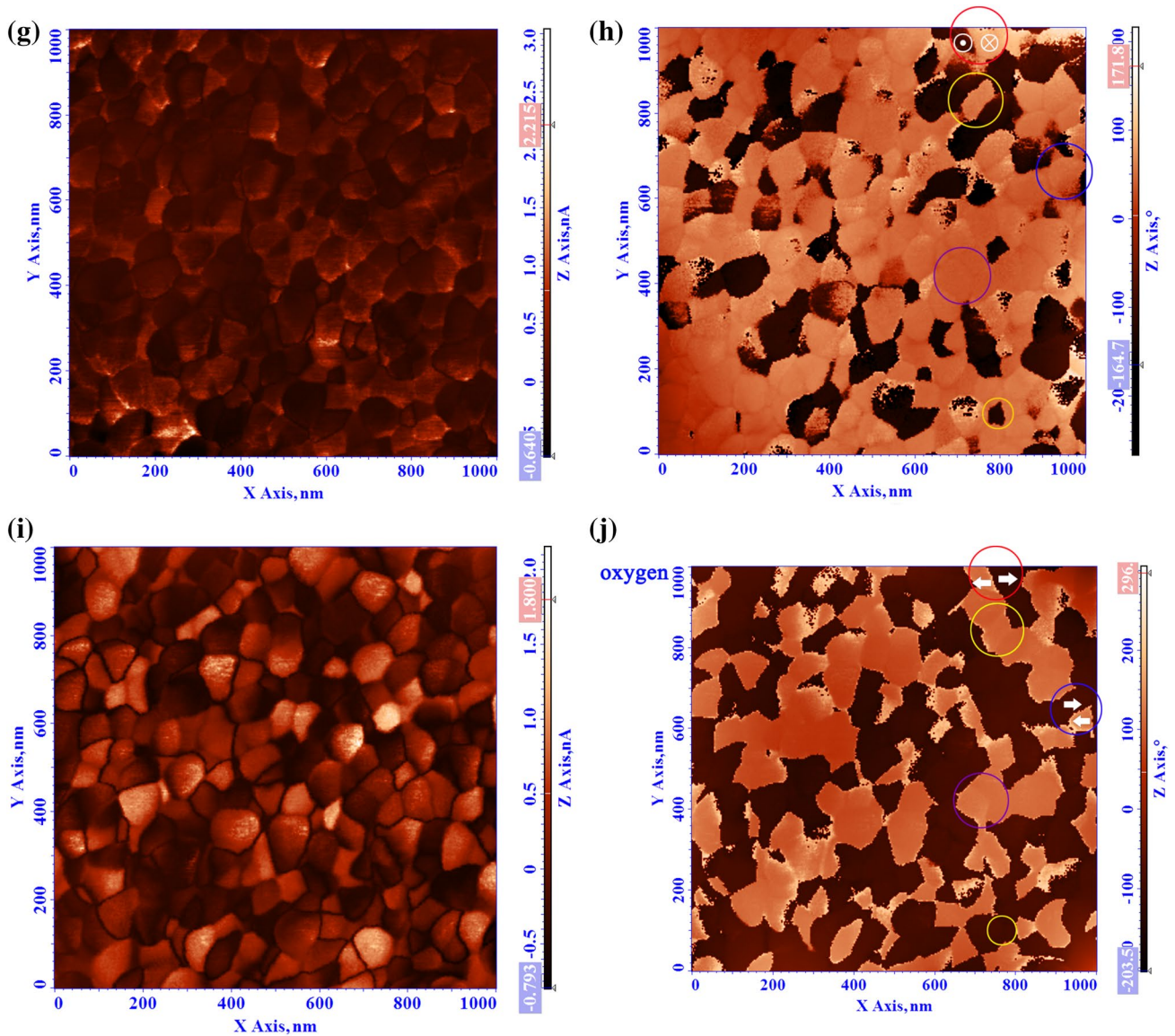


**Fig. 5** (continued)

**Acknowledgements** This work was supported by the National Natural Science Foundation of China (Grant Nos. 51102288, 51372283, 51402031, 61404018) and the Program for Innovation Teams in University of Chongqing, China (Grant No. CXTDX201601032).

## References

1. X. Yang, Z. Zhou, T. Nan, Y. Gao, G.M. Yang, M. Liu, N.X. Sun, *J. Mater. Chem. C* **4**, 234 (2016)
2. S. Dong, J.M. Liu, S.W. Cheong, Z.F. Ren, *Adv. Phys.* **64**, 519 (2015)
3. J. Scott, *NPG Asia Mater.* **5**, e72 (2013)
4. D. Sando, Y.R. Yang, E. Bousquet, C. Carrétéro, V. Garcia, S. Fusil, D. Dolfi, A. Barthélémy, P. Ghosez, L. Bellaiche, M. Bibes, *Nat. Commun.* **7**, 10718 (2016)
5. A. Solmaz, M. Huijben, G. Koster, R. Egoavil, N. Gauquelin, G.V. Tendeloo, J. Verbeeck, B. Noheda, G. Rijnders, *Adv. Funct. Mater.* (2016). doi:[10.1002/adfm.201505065](https://doi.org/10.1002/adfm.201505065)
6. L.V. Costa, L.S. Rocha, J.A. Cortés, M.A. Ramirez, E. Longo, A.Z. Simões, *Ceram. Int.* **41**, 9265 (2015)
7. M.S. Bernardo, T. Jardiel, M. Peiteado, A.C. Caballero, M. Villegas, *J. Eur. Ceram. Soc.* **31**, 3047 (2011)
8. T. Zheng, J.G. Wu, *J. Mater. Chem. C* **3**, 11326 (2015)
9. C.H. Yang, P.P. Lv, J.H. Song, J.F. Leng, X.S. Sun, *J. Mater. Sci.* **28**, 3423 (2017)
10. G.H. Dong, G.Q. Tan, W.L. Liu, A. Xia, H.J. Ren, *Ceram. Int.* **40**, 1919 (2014)
11. S.S. Rajput, R. Katoch, K.K. Sahoo, G.N. Sharma, S.K. Singh, R. Gupta, A. Garg, *J. Alloy Compd.* **621**, 339 (2015)
12. H.Z. Chen, M.C. Kao, S.L. Young, J.D. Hwang, J.L. Chiang, P.Y. Chen, *J. Magn. Magn. Mater.* **381**, 127 (2015)
13. P.P. Lv, X.M. Jiang, J. Yan, G.D. Hu, *J. Mater. Sci.* **28**, 2233 (2017)



14. W.L. Zhou, H.M. Deng, H.Y. Cao, J. He, J. Liu, P.X. Yang, J.H. Chu, *Mater. Lett.* **144**, 93 (2015)
15. C.C. Leu, T.J. Lin, S.Y. Chen, C.T. Hu, *J. Am. Ceram. Soc.* **98**, 724 (2015)
16. S. Hussain, S.K. Hasanain, G. Hassnain Jaffari, S. Shah Ismat, *Curr. Appl. Phys.* **15**, 194 (2015)
17. S.M. He, G.L. Liu, D.P. Zhu, S.S. Kang, Y.X. Chen, S.S. Yan, L.M. Mei, *Chin. Phys. B* **23**, 036801 (2014)
18. Y.H. Chu, T. Zhao, M.P. Cruz, Q. Zhan, P.L. Yang, L.W. Martin, M. Huijben, C.H. Yang, F. Zavaliche, H. Zheng, R. Ramesh, *Appl. Phys. Lett.* **90**, 252906 (2007)
19. C.J. Cheng, C.L. Lu, Z.H. Chen, L. You, J.L. Wang, T. Wu, *Appl. Phys. Lett.* **98**, 242502 (2011)
20. H.Y. Go, N. Wakiya, H. Funakubo, K. Satoh, M. Kondo, J.S. Cross, K. Maruyama, N. Mizutani, K. Shinozaki, *Jpn. J. Appl. Phys.* **46**, 3491 (2007)
21. K. Prashanthi, M. Gupta, Y.Y. Tsui, T. Thundat, *Appl. Phys. A* **110**, 903 (2013)
22. V.R. Singh, A. Dixit, A. Garg, D.C. Agrawal, *Appl. Phys. A* **90**, 197 (2008)
23. H.Y. Liu, Y.P. Pu, X. Shi, Q.B. Yuan, *Ceram. Int.* **39**, S217 (2013)
24. A.Z. Simões, C.S. Riccardi, M.L. Dos Santos, F. González García, E. Longo, J.A. Varela, *Mater. Res. Bull.* **44**, 1747 (2009)
25. J.W. Kim, C.M. Raghavan, D. Do, T.K. Song, S.S. Kim, *Integr. Ferroelectr.* **132**, 39 (2012)
26. S.K. Singh, N. Menou, H. Funakubo, K. Maruyama, H. Ishiwara, *Appl. Phys. Lett.* **90**, 242914 (2007)
27. W. Cai, C.L. Fu, J.C. Gao, H.Q. Chen, *J. Alloy Compd.* **480**, 870 (2009)
28. J.W. Zhai, X. Yao, J. Shen, L.Y. Zhang, H. Chen, *J. Phys. D Appl. Phys.* **37**, 748 (2004)
29. Q.L. Zhao, P.P. Tan, G.P. He, J.J. Di, D.W. Wang, L.H. Qi, H.B. Jin, M.S. Cao, *J. Sol-Gel Sci. Technol.* **78**, 258 (2016)
30. D. Lee, B.C. Jeon, A. Yoon, Y.J. Shin, M.H. Lee, T.K. Song, S.D. Bu, M. Kim, J.S. Chung, J.G. Yoon, T.W. Noh, *Adv. Mater.* **26**, 5005 (2014)